Journal of the European Ceramic Society **18** (1998) 39–49
Published by Elsevier Science Limited

PII: S0955-2219(97)00103-9
0955-2219/98/$19.00 + 0.00

Microstructural Characterization of Al_2O_3–SiC Nanocomposites

H. K. Schmid, M. Aslan, S. Assmann, R. Naß and H. Schmidt

Institut für Neue Materialien, Im Stadtwald 43, D-66123 Saarbrücken, Germany

(Received 6 January 1997; accepted 18 April 1997)

Abstract

Al_2O_3 composite ceramics containing 10 vol% SiC nanoparticles were prepared by pressureless sintering. SiC particles < 150 nm detach from the matrix grain boundaries during grain growth and are predominantly observed in intragranular positions, whereas larger SiC particles retain intergranular positions. Thermal expansion mismatch causes local residual tensile stresses in the matrix grains, giving rise to strain contrasts in TEM imaging; occasionally microcracking around intragranular inclusions ⩾100 nm is observed in thin TEM foils. It appears that the volume fraction of intragranular SiC particles in the size range 100 < d < 150 nm should not exceed ≈0·5% in high strength/high toughness Al_2O_3–SiC nanocomposites. The interaction between propagating cracks and internal stress fields around intragranular inclusions forces a transgranular fracture mode. Grain boundary pinning by large intergranular SiC particles, in combination with solute drag inhibits matrix grain growth, while the presence of an amorphous phase at Al_2O_3 grain boundaries and Al_2O_3–SiC phase boundaries assists in densification. Excess liquid phase is exuded from the interfaces during consolidation and accumulates in large pores, stabilized by the accidental agglomeration of large SiC particles. Published by Elsevier Science Limited.

1 Introduction

The dispersion of second-phase particulates in ceramic matrix composites could result in considerable improvements in mechanical properties, and thus offers possibilities to overcome the inherently low fracture toughness of ceramic materials.[1,2] In recent years there has been a growing interest in nanocomposites, in which ceramic matrices are reinforced by the dispersion of inert sub-μm-sized particles. In particulate ceramic–ceramic composite systems the increase in fracture toughness could be attributed to the interaction between propagating macrocracks and local stress fields around inclusions; various toughening mechanisms due to microcracking, crack tip shielding, crack branching, and crack deflection have been proposed.[1,3,4]

Significant improvements in strength and fracture toughness have been reported for SiC dispersed Al_2O_3 composites.[5] In this system the location of second phase particles within the Al_2O_3 matrix, i.e. intragranular versus intergranular positions is a critical factor; it appears to be strongly dependent on the initial size of the SiC particles and the choice of starting materials.[5–8] The dilatation of crack propagation may arise because microcracking relieves local residual tensile stresses in the matrix, caused by the thermal expansion mismatch. Though the initially reported gain in fracture toughness in Al_2O_3–SiC composites could not be reproduced,[9,10] any improvements in fracture toughness should probably be attributed to a change from intergranular to transgranular fracture mode; however, some controversy on possible toughening mechanisms still exists.[11,12]

The presence of SiC nanoparticles effectively inhibits grain growth in the Al_2O_3 matrix phase; this may result in a fine-grained composite exhibiting improved strength.[7,13] However, the dispersion of an inert second phase may have detrimental effects on the densification of particulate ceramic composites,[7,14–16] and often hot-pressing is required to achieve dense compacts. By carefully balancing these beneficial and detrimental effects, fabrication of high strength/high toughness nanocomposites with densities >98% theor. appears to be achievable by pressureless sintering.[6] Therefore, understanding the dispersion behavior of SiC nanoparticles and their role in the microstructural evolution is of fundamental importance for the optimization of Al_2O_3–SiC nanocomposites. In this class of materials, properties are to a large extent

controlled by the structure of internal interfaces, i.e. phase- and grain- boundaries. Often glassy residual intergranular phases exist from interreactions between constituent phases, dopands and impurities present in the starting materials, and may assist in densification. Hence detailed investigations on the structure of interfaces, involving structural and microchemical analysis with high spatial resolution by means of analytical transmission electron microscopy (AEM) are required. The motivation behind these investigations is to understand the mechanisms responsible for the strengthening and toughening observed in SiC dispersed Al_2O_3 ceramics. In the present work, two Al_2O_3–SiC nanocomposites were characterized by AEM techniques. Emphasis is put on the dispersion behavior of SiC inclusions, and their role in the formation of residual intergranular phases and resulting microstructural evolution during processing of these nanocomposite ceramics.

2 Experimental Details

Two Al_2O_3–SiC composite materials have been manufactured from commercially available α-Al_2O_3 (AKP 53, Sumitomo / Japan), and α-SiC (UF 45, H.C. Starck/Germany) powders. The starting powders are characterized by their range of particle sizes $d = 100 \div 400$ nm, $d_{50} = 220$ nm, specific surface area $\gamma = 12{\cdot}5\ m^2\,g^{-1}$ for Al_2O_3; and $d = 50 \div 500$ nm, $d_{50} = 120$ nm, $\gamma = 45\ m^2\,g^{-1}$ for SiC, respectively. The starting SiC powder also contained a small fraction of free carbon (0·55 wt%) as well as 6 wt% oxygen due to surface oxidation as a result of powder handling in ambient air. Al_2O_3 powder was mixed with SiC (10 vol%) in H_2O and sintered in N_2 at $T = 1970$ K for $t = 4$ h (sample material A: relative density $\rho = 96{\cdot}1\%$ theor.), and $T = 2120$ K for $t = 1$ h (material B: $\rho = 98{\cdot}7\%$ theor.), respectively.

Thin self-supporting electron transparent foils for transmission electron microscopy (TEM) investigations were prepared by standard preparation methods for ceramic materials, i.e. mechanical cutting, dimple grinding/polishing, followed by ion-beam etching (5 keV Ar ions, 12° angle of incidence). The samples were examined in an analytical TEM (Philips CM 200 FEG) operated at 200 kV acceleration voltage. The AEM was equipped with an energy-dispersive X-ray spectrometer (EDS) attachment for chemical microanalysis (EDAX DX 4 with SUTW detector), and cooled slow-scan CCD camera (Gatan 694 SSC) for image recording.

With field emission electron source (FEG) a spatial resolution ≈ 5 nm is achievable in EDS microanalysis in the analytical TEM operated in microprobe mode (30 μm condenser aperture C_1). Under these conditions it may be possible to quantitatively analyze the composition of residual secondary phases situated in isolated pockets $\geqslant 5$ nm in size, while thin intergranular films, typically a few nm thick can be analyzed in a qualitative manner only. Concentration profiles across interfaces were measured qualitatively by using an automated step-scan technique. Though the use of a Si detector with super ultra-thin window (SUTW) enables the detection of light elements $Z \geqslant 6$ in EDS analysis, the criterion for the thin film approximation [$\chi\rho t < 0{\cdot}1$; where χ^i is the mass absorption coefficient of the sample for the X-ray line of element (i), and ρ, t are the sample density and thickness, respectively] is usually not met by the light elements $Z < 12$, thus rendering an absolute quantification particularly of C and O concentrations rather unreliable by standardless analysis. To avoid electrical charging, samples were coated with a thin film of amorphous C for TEM imaging; some EDS analyses were carried out on uncoated samples in order to assess true C concentrations in the sample material. Relative concentrations of Al and Si cation constituents were estimated from the integrated intensity ratios of the Al–K and Si–K lines using calculated values for the K_{AB} factors ($K_{Al,\,Si} = 0{\cdot}95$). For the light elements C and O, K_{AB} factors were determined experimentally using thin sections of the crystalline phases Al_2O_3 and SiC as internal standards ($K_{O,\,Si} = 3{\cdot}3$; $K_{C,\,Si} = 3{\cdot}6$). By using these K_{AB} factors in quantification, relative errors $< 10\%$ could be achieved in specimen areas ≈ 40 nm thick. In thicker foils systematic errors due to increasing X-ray absorption effects particularly of C–K and O–K are encountered, while in very thin sections counting statistics for X-rays from light elements are poor due to a decrease in interaction volume and inherently low X-ray fluorescence yields.

3 Results

The microstructure and microchemistry of SiC-dispersed alumina composite ceramics have been investigated by conventional and analytical TEM techniques. The microstructure typically observed in these materials is shown in Fig. 1 (TEM bright-field image). SiC particles of approximately spherical shape ranging in diameter between ≈ 20 and 150 nm are situated predominantly in intragranular positions. Small SiC particles appear to be either perfect single crystals or show micro-twinning characteristic of stacking sequence faults in polytypoid structures as seen in high resolution images

Fig. 1. Microstructure of Al_2O_3–SiC nanocomposite: SiC particles $\leqslant 150$ nm situated in intragranular positions; microcracks indicated by arrows (TEM-BF image; material A).

(Fig. 2). SiC particles in intragranular positions give rise to strain contrasts in the surrounding Al_2O_3 lattice. Under dynamic (Bragg) imaging conditions these strain contrasts are visible in TEM images and are clear indications of the presence of residual internal stresses in the matrix grains (Fig. 2). Occasionally, microcracks have been observed in the vicinity of intragranular spherical SiC inclusions with diameters in the range $100 < d < 150$ nm. These microcracks extend radially from the particle surfaces into the surrounding Al_2O_3 matrix up to ≈ 200 nm in length (indicated by arrows in Fig. 1). Particles with diameters $\geqslant 200$ nm usually are more irregularly shaped and are situated exclusively in intergranular positions (Fig. 3). The large intergranular SiC particles tend to form clusters in association with open macropores and pockets of an amorphous secondary phase, as was frequently observed in these materials (Figs 4 and 5).

3.1 Intergranular phase

High angle grain boundaries in liquid-phase-sintered ceramics are usually wetted by a thin film of a vitreous intergranular phase.[17,18] A detailed view of the structure of internal interfaces is shown in Fig. 6. The TEM-BF images show a SiC particle, approx. 150 nm in size, situated in an intergranular position. Sections of both the Al_2O_3–SiC phase boundary (ASPB) as well as the Al_2O_3 grain boundary (AGB) are viewed in edge-on orientation, i.e. with boundary planes parallel to the incident electron beam. In out-of-focus imaging conditions these boundaries give rise to Fresnel fringe contrasts due to discontinuities in the inner

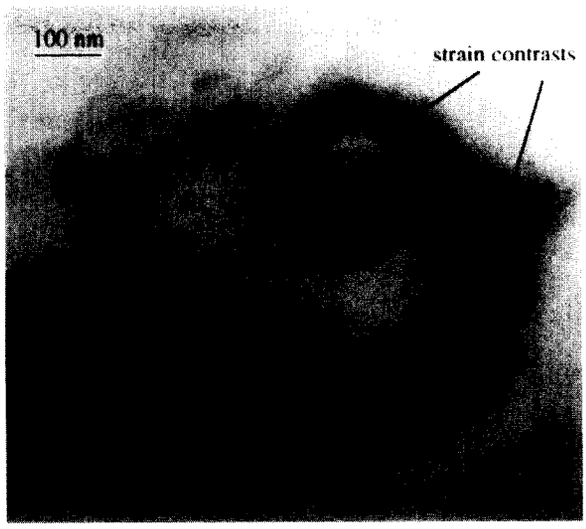

(a)

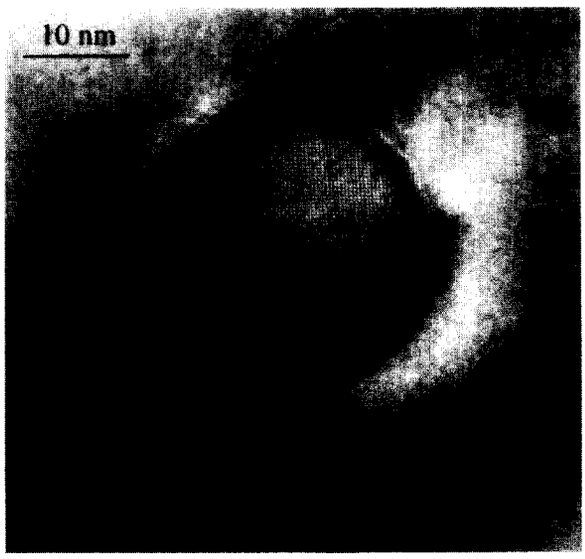

(b)

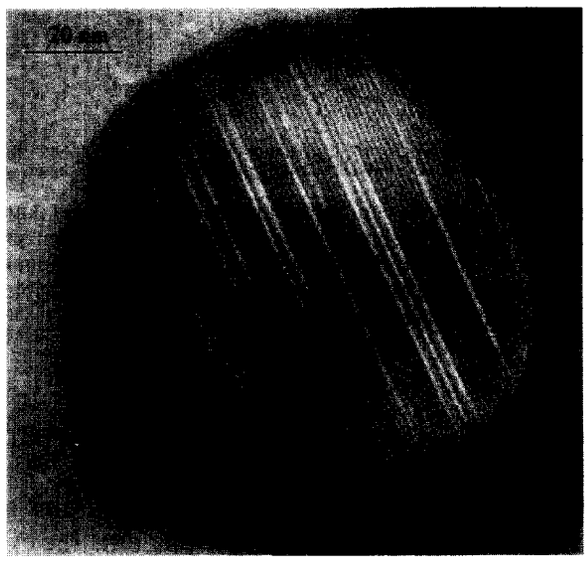

(c)

Fig. 2. SiC particles in intragranular positions: (a) strain contrasts around SiC inclusion, SiC particles not in Bragg orientation give rise to weak amplitude contrasts; (b) structure imaging of small unfaulted SiC inclusion, (c) microtwins in polytype structure.

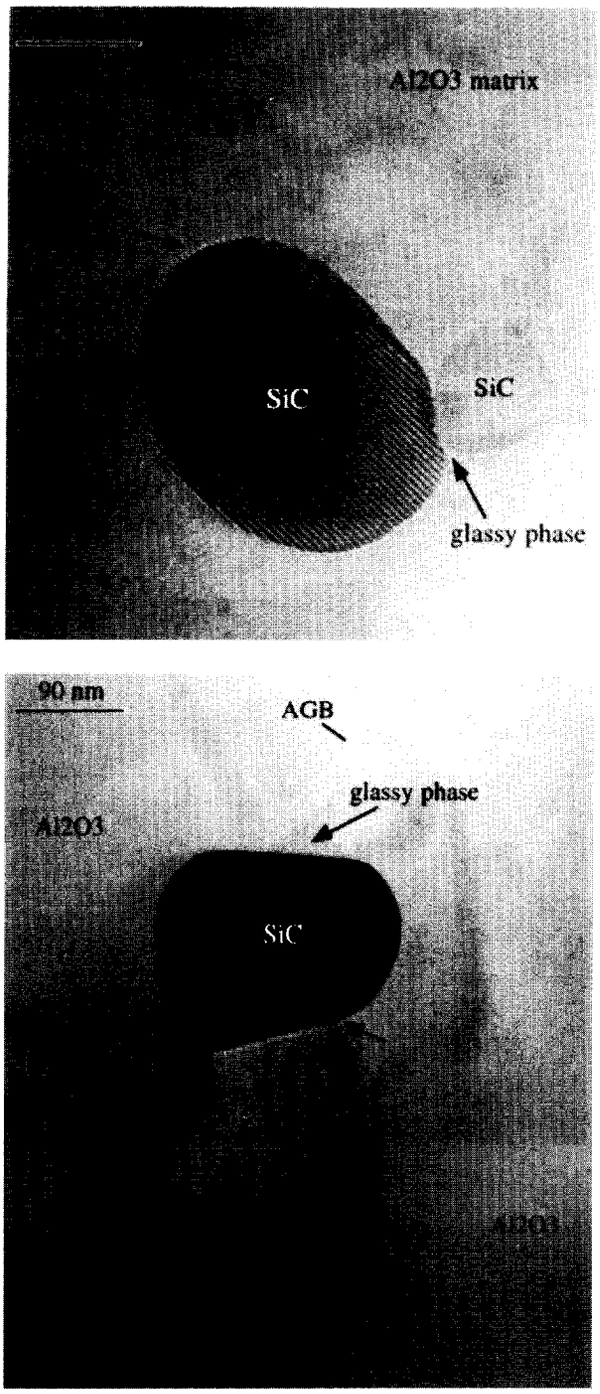

Fig. 3. SiC particles in intergranular positions: (a) lattice fringe image of 0001 base planes (6H,α-SiC) in medium-sized SiC particle, (b) two SiC particles at Al_2O_3 grain boundary; small pockets of liquid phase (marked by arrows) are visible in neck areas and triple grain junctions (material B).

potential of the lattice, and are an indication of the presence of secondary intergranular films.[19] In favorable circumstances, where adjacent grains are in suitable orientations for lattice imaging, the existence of thin intergranular films may be revealed by high resolution TEM imaging of interfaces in exact edge-on orientation.

Figure 7 shows large SiC particles in intergranular positions; SiC–Al_2O_3–SiC triple grain junction areas (TJ) are shown in detail in the high resolution images of material A [Fig. 7(a)], and material B [Fig. 7(b)]. Those sections of interfaces viewed in edge-on orientation unambiguously revealed the presence of thin intergranular films. From high resolution imaging it appears that amorphous intergranular films of uniform thickness ≈0·9 nm thick are present at both the Al_2O_3 grain boundaries and Al_2O_3–SiC phase boundaries, whereas the intergranular phase at SiC grain boundaries appears to be even thinner and discontinuous, in accordance with theoretical predictions.[18] In general, there are no large pockets of excess intergranular phase observed at triple grain junctions

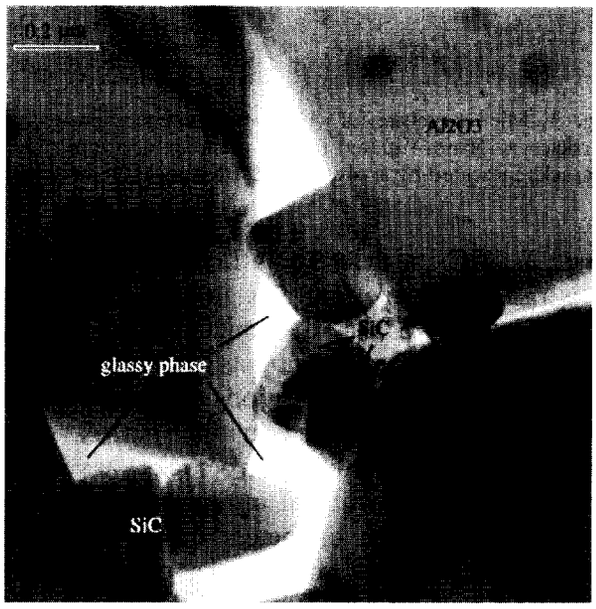

(a)

(b)

Fig. 4. Agglomerates of large intergranular SiC particles: (a) agglomerated SiC particles (≥ 200 nm), and pockets of glassy phase in intergranular position, (b) large number of SiC particles agglomerated around open macropore (material B).

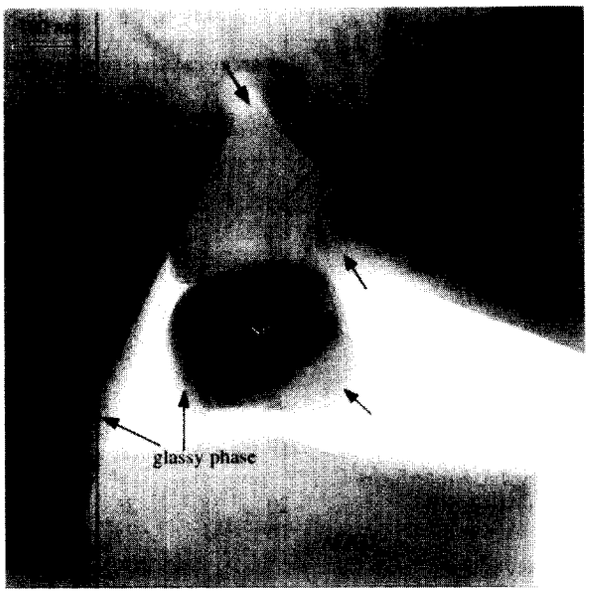

(a)

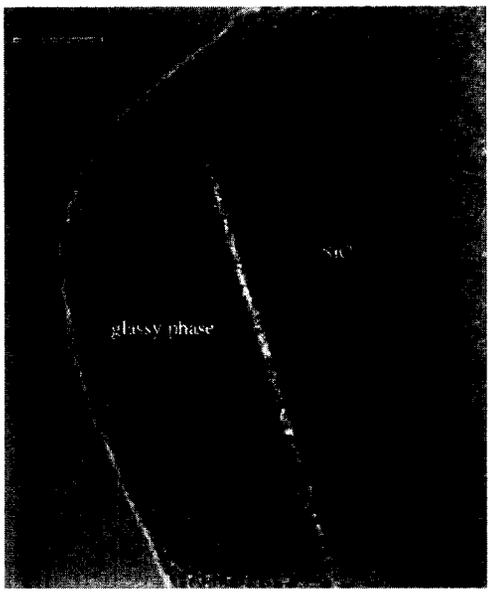

(b)

Fig. 5. (a) Large SiC particles agglomerated in pore area show rim of residual glassy phase; (b) high resolution image of solid–liquid interface (material B).

(e.g. Fig. 6). Only in areas where the agglomeration of large irregularly shaped SiC particles in intergranular positions prevented a complete densification, the open pores between particles acted as sinks for the accumulation of excess amorphous phase in large pockets (Figs 4 and 5).

3.2 Microanalysis

Bulk compositions of the constituent phases, i.e. Al_2O_3 matrix and SiC inclusions were measured by EDS analysis in TEM microprobe mode on a large number of individual particles. For the light elements C and O the K_{AB} factors were determined from the intensity ratios C–K/Si–K and O–K/Si–K measured in sections ≈ 50 nm thick in Al_2O_3 and SiC, respectively. Since no corrections were made for unavoidable absorption effects (thin film approximation), light elements C and O are overestimated in very thin sample areas $< < 50$ nm, and are underestimated in thick sample areas $> > 50$ nm. Results of EDS analyses of the crystalline constituent phases as well as amorphous residual secondary phase are summarized in Table 1; normalized relative concentrations are

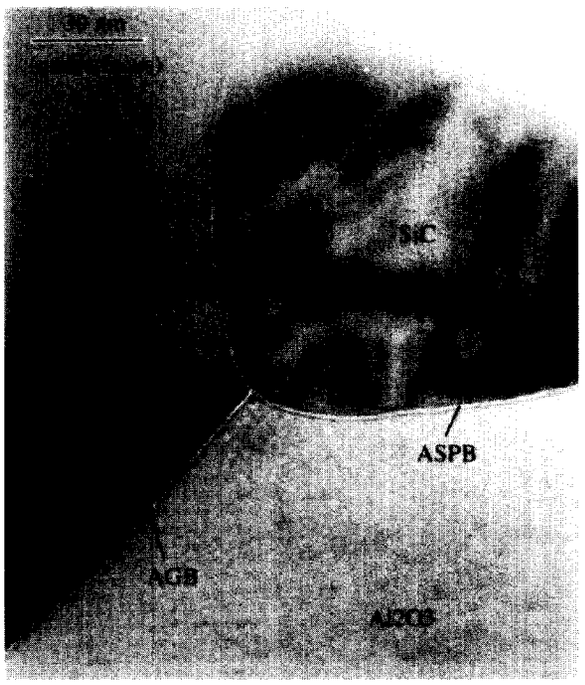

(a)

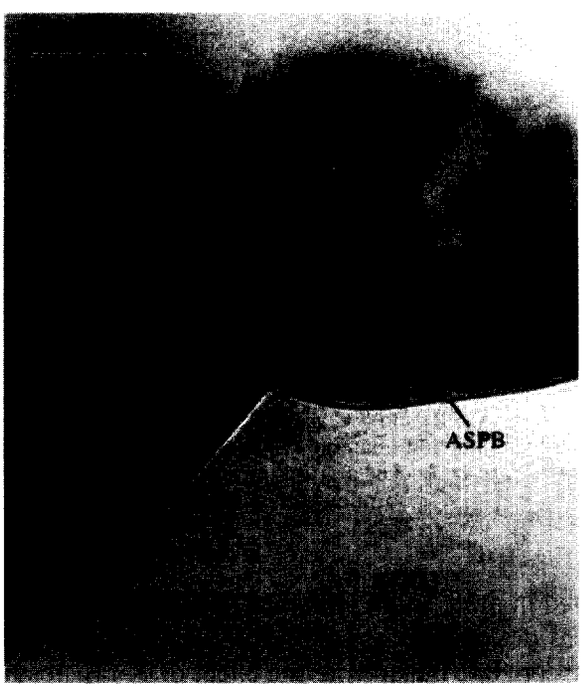

(b)

Fig. 6. Al_2O_3 grain boundary (AGB) and Al_2O_3–SiC phase boundary (ASPB) viewed edge-on showing Fresnel fringe contrasts at (a) under-focused, and (b) over-focused conditions.

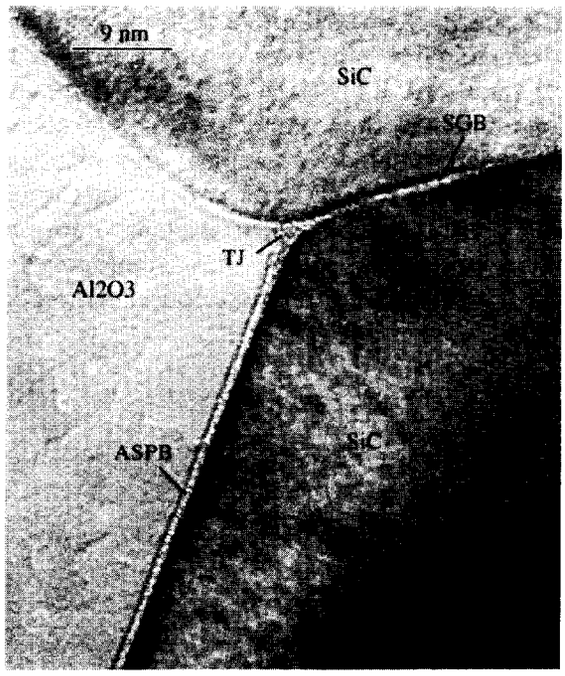

(a)

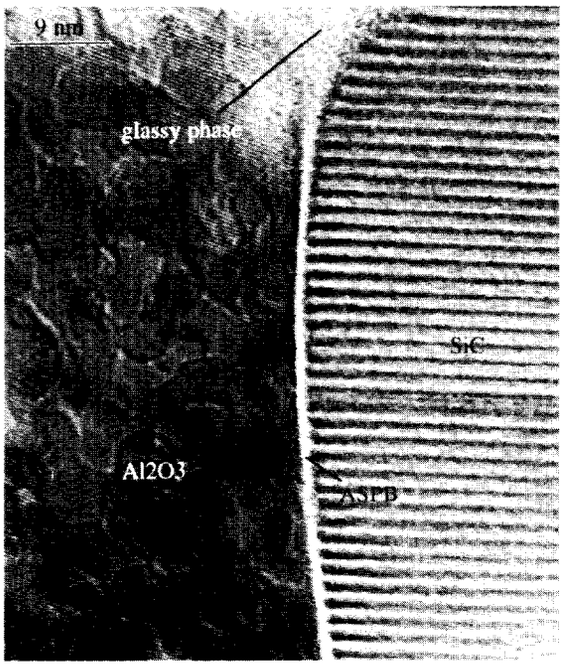

(b)

Fig. 7. High resolution TEM images showing vitreous intergranular films at internal interfaces. (a) Al_2O_3–SiC phase boundary (ASPB) and SiC grain boundary (SGB) adjacent to triple grain junction (material A), and (b) ASPB in material B; glassy phase in pocket at triple grain junction gives rise to amorphous phase contrast.

listed in at%. In SiC (feature A) spectra (1) and (2) were determined in small and large SiC particles, respectively, illustrating the effect of X-ray absorption on measured apparent relative concentrations of C and O, while spectrum (3) lists a set of data determined by averaging the results of 15 individual analyses. This method of multiple-spectra analyses [20] allows substantial improvements on the

Table 1. EDS microanalysis in Al_2O_3–SiC composites

	Apparent relative concentrations (at%)			
Feature	*C*	*O*	*Al*	*Si*
(A) SiC particle				
Small particle (≈25 nm)	52	4	1	43
Thick region (≈100 nm)	41	3	1	55
Average value	46	5·5	1·4	46·5
(B) Al_2O_3 matrix				
Thin section (≈30 nm)	2	60	38	0·6
Average value	3	56	41	<0·1
(C) Grain boundaries				
SiC GB region	37	8	4	51
Al_2O_3 GB region	10	55	33	2
(D) Interphase interfaces				
SiC–Al_2O_3 PB	20	38	26	16
SiC–Al_2O_3 TJ	16	41	29	14
(E) Glassy phase				
Large pocket	12	38	17	33
Rim at SiC particle	16	43	19	22
Rim at Al_2O_3 grain	13	53	29	3
Thin glass section	18	20	8	54

accuracy and reliability of EDS microanalysis; wherever possible, data sets listed in Table 1 are averaged values from 10 to 15 measurements.

An attempt was made to investigate the segregation behavior of the constituent elements on internal interfaces. Results of the EDS spot analyses indicated a clear trend towards increased relative concentrations of Al and O in the regions of SiC grain boundaries adjacent to triple grain junctions, while C and to a lesser extent also Si concentrations on Al_2O_3 grain boundaries are found to be increased in comparison with bulk SiC and Al_2O_3, respectively (Table 1, feature C). Line scans across Al_2O_3 grain boundaries clearly revealed an increase in the Si–K count rate, and thus an increased relative Si concentration in the grain boundary region, as shown in Fig. 8(a). Analyses at SiC–Al_2O_3 triple grain junctions and along phase boundaries (feature D) yielded mixed apparent concentrations of all constituent elements due to considerable phase overlap in the sampling volume.

EDS spectra determined from a large number of pockets of glassy phase revealed that the amorphous phase is very inhomogeneous in composition (feature E).Some regions in large pockets were found to be rich in Si, while others showed rather low Si contents but high Al and/or O concentrations. From TEM observations it appears that spaces between large SiC particles agglomerated in intergranular positions are either completely or partially filled by amorphous phase; in the latter case a rim ≈20 nm wide of residual glass phase is observed along the edges of crystalline phases (Fig. 5). Glassy seams on Al_2O_3 grains appear to be essentially amorphous Al oxide (Spectrum 3),

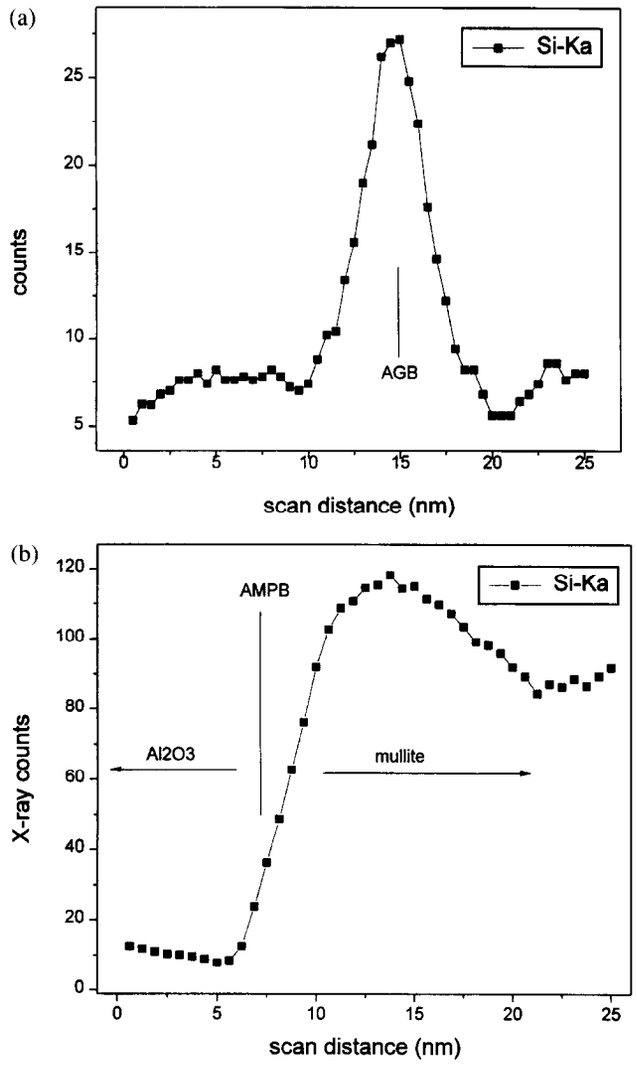

Fig. 8. Composition profiles across internal interfaces (automated step scans): (a) Si–K_α signal across Al_2O_3 grain boundary (AGB); (b) Si–K_α signal across Al_2O_3–mullite phase boundary (AMPB).

while the glassy phase on SiC particles (Spectrum 2) as well as other glassy bodies appear to be alumino-silicates of varying composition.

All EDS spectra have been checked for a possible presence of residual N impurities from the sintering atmosphere. It appears from the EDS analysis that no detectable N-containing phase exists in these materials. Occasionally, small pockets of secondary phases, identified as mullite and a crystalline Si-rich phase were observed in coexistence with the alumino-silicate melt. The analysis by X-ray diffraction (XRD) on bulk samples of these composite materials failed to detect these minor secondary phases.

4 Discussion and Conclusions

The principal features of microstructure which have developed in Al_2O_3–SiC composite ceramics are a consequence of the dispersion behavior of SiC particles, and the formation of secondary intergranular phases by interreactions between constituent phases and SiO_2 impurities. The principal microstructure observed in both materials A and B consists of pure SiC particles dispersed in the Al_2O_3 matrix. The SiC particles $\leqslant 150$ nm dia. are situated in intragranular positions inside the Al_2O_3 matrix grains, while larger SiC particles > 150 nm are observed in intergranular positions at grain boundaries and multi-grain junctions. Matrix grains measured by the linear intercept method in SEM images yielded mean grain sizes of $\approx 2{\cdot}2\,\mu$m (material A), and $\approx 3{\cdot}9\,\mu$m (material B), respectively. This indicates an increase in particle size by approximately one order of magnitude in the matrix phase, while the mean particle size of SiC inclusions appears to have remained unchanged ($d_{50} \approx 120$ nm). By comparing the microstructure observed in these nanocomposite materials with that of undoped Al_2O_3 ceramics sintered at comparable conditions,[6] it is obvious that the SiC inclusions significantly inhibited grain growth in the Al_2O_3 matrix. Since the force exerted by an intergranular inclusion on a moving grain boundary can be assumed to be proportional to its size,[21] small particles detach from advancing grain boundaries during grain growth and become entrapped inside the matrix grains, while grain boundaries are effectively pinned by the large SiC particles in intergranular positions. These observations indicate that the growth rate of matrix grains exceeds the dissolution and reprecipitation rates at contact areas of spherical inert inclusions even in systems where thin vitreous intergranular films provide paths for rapid material transport by fast diffusion along internal interfaces.[22,23] The mobility of internal interfaces, irrespective of being wetted by a thin film of residual intergranular phase can be rate limited by solute drag, which is controlled by lattice diffusion.[24] Thus, the reduced grain growth observed in the matrix phase in comparison with that of undoped Al_2O_3 ceramics is a result of both grain boundary pinning by large SiC particles in intergranular positions, and solute drag exerted by solutes segregated to internal interface regions. Very limited data are available on mutual solid solubility between Al_2O_3 and SiC in the temperature range $T \leqslant 2120$ K, as well as on the solubility of SiC in alumino-silicate melts.[25] EDS spectra from Al_2O_3 matrix grains showed Si concentrations at low levels < 1 at%, while spectra taken from large SiC inclusions, protruding over the edge of the thinned sample so that phase overlap is minimized, yielded Al concentrations between 1 and 2 at% (Table 1). However, because of unavoidable collection of X-ray signals generated

by electrons scattered into sample areas beyond the lateral resolution limit of ≈ 5 nm in microanalysis cannot be ruled out,[26] it appears that a mutual solubility limit at the 1 at% level can be assumed in accordance with reports on Al-containing liquid-phase sintered SiC.[27,28]

In the consolidated state both crystalline constituent phases are in contact with an amorphous intergranular phase situated in thin films at internal interfaces and small pockets at multiple grain junctions. The starting SiC powder contained 0·55 wt% free C and 6 wt% O, the latter in form of an SiO_2 surface oxide layer. With a specific surface area of 45 $m^2 g^{-1}$, the O content relates to a surface density of 0·0025 g SiO_2 m^{-2}, which corresponds to an SiO_2 surface layer ≈ 1 nm thick. Since in the Si–Al–C–O system Al_2O_3 is thermodynamically more stable as compared to that of SiO_2, gaseous products resulting from the reaction

$$SiC + 2SiO_2 \rightarrow 3SiO_{(g)} + CO_{(g)} \qquad (1)$$

may form for low C/SiO_2 ratios and slow heating rates, while all of the free C is converted to SiC above 1840 K.[25] Depending on the reaction kinetics, a transient eutectic alumino-silicate melt can form by SiO_2 reacting with Al_2O_3 at $T > 1860$ K[29] at fast heating rates during the sintering process. In the temperature range $1860 \leqslant T \leqslant 2140$ K, the three crystalline phases SiC, Al_2O_3 and mullite (3 $Al_2O_3 \cdot 2$ SiO_2) are thermodynamically stable in coexistence with the eutectic melt. Mullite has been observed as a minor phase only in small pockets in these materials, which may be due to the slow rate expected for the reaction of Al_2O_3 with SiO_2-rich glassy phase during mullite formation.[30] EDS analyses showed that the glassy phase in large pockets is indeed SiO_2-rich (Al/Si ratio < 3), albeit in a non-equilibrium state as expressed by its highly nonhomogeneous composition which may be attributed to the partial loss of gaseous reaction products during sintering. Most of the liquid phase is exuded from the interfaces during the sintering process and accumulated in large pockets in porous regions, while little is retained in thin intergranular films and small pockets at triple grain junctions. Theoretical considerations predict, and high resolution TEM observations have confirmed that vitreous intergranular films in ceramic systems have an equilibrium thickness.[18] In the Al_2O_3–SiO_2 system a siliceous intergranular phase ≈ 2 nm thick is predicted, while in SiC the Van der Waals attraction exceeds the disjoining forces and no continuous intergranular phase is expected. This is in accordance with our observations of continuous intergranular films at Al_2O_3 grain boundaries and Al_2O_3–SiC phase boundaries between matrix and intergranular particles, whereas in the case of SiC grain boundaries, Al and O is detected in low concentrations only in some grain boundary regions adjacent to triple grain junctions.

Concentration gradients across internal interfaces may arise from segregation involving diffusion of mobile solutes. A space charge arises at any geometric discontinuity, such as internal interfaces, including solid-liquid phase boundaries at two-grain junctions wetted by an intergranular phase.[24] Thus, the segregation behavior of solutes on wetted interfaces should not be principally different from that of, 'clean' crystalline grain boundaries. Since grain boundaries in Al_2O_3 carry a positive charge,[31] tetravalent Si solutes, with an effective charge of $(+1)$ and small misfit strain, usually show little tendency towards segregation on Al_2O_3 grain boundaries,[32] whereas for Al solutes, occupying Si sites in SiC,[28] and carrying an effective charge of (-1), a tendency towards segregation at SiC grain boundaries would be expected.

The oxygen concentration in excess of an atom ratio $O/Al = 1{\cdot}5$ measured in SiC grain boundary regions adjacent to triple grain junctions indicates that at least some SiO_2 could have been retained at these interfaces. In heterogeneous sampling the measured X-ray intensities in EDS analysis are proportional to the convolution product of the electron density distribution function in the electron probe, and the concentration distribution function.[26] Thus, EDS analysis will not reflect the true concentrations in the case of a thin intergranular film of thickness $d << D_{\text{eff}}$ where D_{eff} is the effective probe size (including beam broadening within the foil), because of an dilution effect due to phase overlap from adjacent grains,[23,26] and true O concentrations in SiC grain boundaries could actually exceed apparent measured values. The presence of a siliceous intergranular film at Al_2O_3 grain boundaries (AGB) has also been confirmed by Si concentration profiles measured across interfaces in edge-on orientations [Fig. 8(a)]. Though all Si atoms in these boundaries may be located within the thin intergranular film (≈ 1 nm), measured profiles show a width ≈ 5 nm (FWHM), which is to the order of the probe size dominating the convolution product. Profiles of Si concentration across Al_2O_3–mullite phase boundaries (AMPB), on the other hand, showed a considerably broader maximum ≈ 12 nm wide on the mullite side of the interface region [Fig. 8(b)], indicating a tendency for Si to segregate at AMPBs in mullite.

Despite the confirmation of the existence of an intergranular phase at Al_2O_3 grain boundaries by the observation of Fresnel fringe contrasts, high resolution imaging, as well as EDS analysis, some

ambiguity may still exist due to possible artifacts from specimen preparation.[17] The high C concentration at ratios C/Si > > 1 observed at Al_2O_3 grain boundaries and other interfaces could be caused by surface grooving during ion milling resulting in excessive surface deposition of C in grain boundary regions.

Only a small fraction of the amorphous phase is retained in thin films at the interfaces. All liquid phase in excess of the equilibrium film thickness, together with possible gaseous products, is exuded from the interfaces in the consolidation process and accumulated in large pockets and pores in the open spaces between large SiC particles agglomerated in intergranular positions. It has been shown that pores coordinated by more than a critical number of grains (usually > 6) are thermodynamically stable.[33] Since no sizeable grain growth is observed in the SiC phase at the sintering temperatures applied to these composites, the number of SiC grains coordinating a large pore is not reduced by grain growth and thus pores will not disappear [Fig. 4(b)]. Their accidental presence in these nanocomposites not only reduces the achievable final density, they also could be critical flaws initiating materials failure and reduce the reliability of structural components. On the other hand, however, the presence of the amorphous intergranular phase may facilitate a liquid phase sintering process at $T > 2030$K, resulting in increased final density of material B ($\approx 98{\cdot}7\%$ theor.) in comparison with material A ($\approx 96{\cdot}1\%$ theor.).

Vitreous intergranular films present at the internal interfaces accommodate the lattice mismatch between Al_2O_3 matrix and SiC inclusions, and facilitate strain relaxation around large SiC particles in intergranular positions by particle rearrangement during the sintering process. However, because of considerable thermal expansion mismatches, radial compressive stresses exist around the SiC inclusions upon cooling. Thus, liquid phase in excess of an equilibrium film thickness is squeezed out from the phase boundaries between matrix grains and singular intergranular SiC inclusions, resulting in strengthened grain boundary structures in well dispersed composites due to a rigid SiC–Al_2O_3 bonding. On the other hand, flaws in the microstructure are introduced in form of large pockets of glassy phase retained in open pores associated with the agglomeration of large SiC particles in intergranular positions.

Considering the intragranular inclusions, it is assumed that SiO_2 impurities, initially present on the surfaces of all SiC particles, are stripped from the intragranular particles during the entrapment process, since a siliceous intergranular phase is hosted preferably by the advancing matrix grain boundaries. Thus, phase boundaries between matrix and intragranular SiC inclusions are assumed to be free of intergranular phase, though unambiguous experimental evidence on the existence of, 'clean' crystalline interfaces might be extremely difficult to obtain by TEM imaging of spherical interfaces. However, from the TEM observations it can be concluded that the absence of an intergranular film inhibits stress relaxation in rigidly bonded Al_2O_3–SiC phase boundaries, resulting in residual compressive stresses in normal direction, and tensile stresses in tangential direction with respect to the interface. The existence of residual lattice strains in Al_2O_3 grains is clearly revealed by the observation of strain contrasts in dynamical TEM imaging. It appears that strain fields extend beyond the interface regions into the surrounding matrix lattice by distances approximately equivalent the particle diameter. Though the size of intergranular inclusions is subcritical for spontaneous microcracking in the alumina/SiC system, microcracks extending radially from SiC inclusions > 100 nm into the surrounding matrix have been observed occasionally in thin TEM foils. It is assumed that the formation of microcracks is most likely initiated in areas where localized high stress concentrations around the largest intragranular inclusions are superimposed by external stresses introduced during thin film preparation for the TEM investigations. If the length of these microcracks is approximately equal to the extent of the internal strain field, as estimated from TEM observations, and assuming a, 'safe' distance between adjacent cracks equal to its length, it is estimated that the volume fraction of intragranular particles > 100 nm should not exceed $\approx 0{\cdot}5$ vol% in order to prevent a decline in strength and fracture toughness under applied external stresses by microcracks linking up with each other. This assumption partly agrees with earlier reports on modest improvements in fracture toughness for SiC fractions < 5 vol%.[11,12] However, it appears from our observations that the volume fraction of intragranular SiC inclusions in the size range $100 < d < 150$ nm may be one of the limiting factors (rather than the total volume of SiC inclusions). It is well known that the fracture toughness can be increased in particulate composite ceramics by controlled microcracking initiated by localized stresses around inclusions, utilizing e.g. the tetragonal → monoclinic transformation in ZrO_2.[1] Similarly, macrocracks propagating in Al_2O_3–SiC nanocomposites interact with the stress fields around intragranularly dispersed SiC inclusions, thus a predominantly transgranular fracture mode is observed in these materials (Fig. 9) as a result of both matrix weakening and grain boundary

Fig. 9. Transgranular macrocrack bridged by large SiC particle in intergranular position causing crack path deflection; position of matrix grain boundary indicated by dashed line (material B, TEM-BF image).

strengthening. Crack branching and crack deflection is observed where macrocracks have traversed microcracked areas, while larger elongated SiC particles in the wake of advancing cracks occasionally facilitate crack-bridging. Creep experiments [9] also suggested much stronger SiC–alumina interfaces in comparison with alumina grain boundaries. Thus, the intergranular dispersion of large SiC inclusions results in reduced grain growth and improved creep resistance by matrix grain boundary pinning, and changing the fracture mode from intergranular (monolithic alumina) to transgranular (SiC–alumina composites). From the TEM observations it appears that singular large SiC particles in intergranular positions do not act as flaws for crack initiation or propagation since stresses are relieved in the presence of liquid intergranular phase during consolidation, whereas rigid agglomerates of large SiC particles resist consolidation. The resulting open pores act as sinks for the accumulation of glassy phase as well as gaseous decomposition products in open pores and thus are critical flaws in the microstructure. The presence of these flaws prevents complete consolidation to near theoretical density and detrimentally affects the mechanical properties, particularly strength and fracture toughness.

In summary, it is concluded from the present TEM studies that both Al_2O_3–SiC nanocomposites under investigation showed similar microstructures. Sintering at 1970 K for 4 h (material A), and 2120 K for 1 h (material B) resulted in final densities of 96·1 and 98·7% theor., and mean grain sizes of $\approx 2{\cdot}2$ and $3{\cdot}9\,\mu$m, respectively. The initial size of the SiC particles is a critical issue for obtaining intragranular particulate composites. Particles $\leqslant 150$ nm detach from advancing grain boundaries and are homogeneously dispersed within the Al_2O_3 matrix grains, whereas larger SiC particles are observed in intergranular positions. As a result of residual internal stresses, microcracking in areas of high stress concentration around intragranular inclusions, and a predominantly transgranular fracture mode is observed. Grain boundary pinning by large SiC particles in intergranular positions together with solute drag effectively control grain growth in the Al_2O_3 matrix. It appears that an optimized nanocomposite requires a carefully balanced size distribution of SiC inclusions, i.e. particles > 150 nm facilitating grain boundary strengthening and controlling grain growth, as well as smaller intragranular particles < 150 nm, where the fraction of particles in the size range $100 < d < 150$ nm should not exceed $\approx 0{\cdot}5$ vol%. Open pores between agglomerated intergranular SiC particles act as sinks for the accumulation of excess liquid phase exuded from the internal interfaces. The removal of agglomerates and the ability to effectively disperse large SiC particles are critical factors for the processing of high strength/high toughness Al_2O_3–SiC nanocomposites.

References

1. Evans, A. G., Perspective on the development of high-toughness ceramics. *Journal of the American Ceramic Society*, 1980, **73**, 187–206.
2. Claussen, N., Microstructural design of zirconia-toughened ceramics (ZTC). In *Advances in Ceramics, Science and Technology of Zirconia II*, Vol. 12., eds. N. Claussen, M. Rühle and A. H. Heuer. American Ceramic Society, Columbus, OH, 1984, pp. 325–351.
3. Hutchinson, J. W., Crack tip shielding by micro-cracking in brittle solids. *Acta Metallurgica*, 1987, **35**, 1805–1819.
4. Rühle, M., Evans, A. G., McMeeking, R. M., Charalambides, P. G. and Hutchinson, J. W., Microcrack toughening in alumina/zirconia. *Acta Metallurgica*, 1987, **35**, 2701–2710.
5. Niihara, K., New design concept of structural ceramic-ceramic nanocomposites. *Journal of the Ceramic Society Japan*, 1991, **99**, 974–982.
6. Aslan, M., Dörr, C., Nass, R. and Schmidt, H., Microstructural development and mechanical properties of pressureless sintered Al_2O_3–SiC composites. In ceramic processing science and technology. *Proceedings of the 5th Internation Conference on Ceramic Processing Science and Technology*, eds. H. Hausner *et al.*, *Ceramic Transactions*, 1995, 51, 665–669
7. Stearns, L. C., Zhao, J. and Harmer, M. P., Processing and microstructure development in Al_2O_3–SiC nanocomposites. *Journal of the European Ceramic Society*, 1992, **10**, 473–477.
8. Piciacchio, A., Lee, S.-H. and Messing, G. H., Processing and microstructure development in alumina-silicon carbide intragranular particulate composite. *Journal of the American Ceramic Society*, 1994, **77**, 2157–2164.
9. Ohji, T., Hirano, T., Nakahira, A. and Niihara, K., Particle/matrix interface and its role in creep inhibition in

alumina/silicon carbide nanocomposites. *Journal of the American Ceramic Society*, 1996, **79**, 33–45.
10. Caroll, L., Sternitzke, M. and Derby, B., Silicon carbide particle size effects in alumina based nanocomposites. *Acta Materialia*, 1996, **44**, 4543–4552.
11. Zhao, J., Stearns, L. C., Harmer, M. P., Chan, H. M., Miller, G. A. and Cook, R. F., Behaviour of alumina-silicon carbide nanocomposites. *Journal of the American Ceramic Society*, 1993, **76**, 503–510.
12. Levin, I., Kaplan, W. D., Brandon, D. G. and Layyous, A. A., Effects of SiC submicrometer particle size and content on fracture toughness of alumina–SiC nanocomposites. *Journal of the American Ceramic Society*, 1995, **78**, 254–256.
13. Borsa, C. E., Jiao, S., Todd, R. I. and Brook, R. J., Processing and properties of Al_2O_3/SiC nanocomposites. *Journal of Microscopy*, 1995, **177A**, 305–312.
14. Weiser, M. W. and De Jonghe, L. C., Inclusion size and sintering of composite powders. *Journal of the American Ceramic Society*, 1988, **71C**, 125–127.
15. Jang, H. M., Rhine, W. E. and Bowen, H. K., Densification of alumina-silicon carbidepowder composites: II, microstructural evolution and densification. *Journal of the American Ceramic Society*, 1989, **72**, 954–958.
16. Lange, F. F., Yamaguchi, T., Davis, B. I. and Morgan, P. E. D., Effect of ZrO_2 inclusions on the sinterability of Al_2O_3. *Journal of the American Ceramic Society*, 1988, **71**, 446–448.
17. Kouh-Simpson, Y., Carter, C. B., Morrissey, K. J., Angelini, P. and Bentley, J., The identification of thin amorphous films at grain-boundaries in Al_2O_3. *Journal of Materials Science*, 1986, **21**, 2689–2696.
18. Clarke, D. R., On the equilibrium thickness of intergranular glass phases in ceramic materials. *Journal of the American Ceramic Society*, 1987, **70**, 15–22.
19. Clarke, D. R., On the detection of thin intergranular films by electron microscopy. *Ultramicroscopy*, 1979, **4**, 33–44.
20. Bonnell, D. A., Rühle, M. and Tien, T.-Y., Redistribution of aluminium ions during processing of sialon ceramics. *Journal of the American Ceramic Society*, 1986, **69**, 623–627.
21. Gladman, T., On the theory of the effect of precipitate particles on grain growth in metals. *Proceedings of the Royal Society London, Ser. A.*, 1990, **294**, 298.
22. Kang, S.-J. L., Kaysser, W. A., Petzow, G. and Yoon, D. N., Growth of Mo grains around Al_2O_3 particles during liquid phase sintering. *Acta Metallurgica*, 1985, **33**, 1919–1926.
23. Schmid, H. K., Pennefather, R., Meriani, S. and Schmid, C., Redistribution of Ce and La during processing of Ce (La)-TZP/Al_2O_3 composites. *Journal of the European Ceramic Society*, 1992, **10**, 381–392.
24. Hwang, S. L. and Chen, I.-W., Grain size control of tetragonal zirconia polycrystals using the space charge concept. *Journal of the American Ceramic Society*, 1990, **73**, 3269–3277.
25. Misra, A. K., Thermochemical analysis of the silicon carbide–alumina reaction with reference to liquid-phase sintering of silicon carbide. *Journal of the American Ceramic Society*, 1991, **74**, 345–351.
26. Schmid, H. K., X-ray microanalysis with high spatial resolution in the AEM. *Proceedings of the Electron Microscopy Society of South Africa*, 1988, **18**, 35–36.
27. Carpenter, R. W., Braue, W. and Cutler, R. A., Transmission electron microscopy of liquid-phase densified SiC. *Journal of Material Research*, 1991, **6**, 1937–1944.
28. Tajima, Y. and Kingery, W. D., Solid solubility of aluminum and boron in silicon carbide. *Journal of the American Ceramic Society*, 1982, **65**, C27.
29. Aksay, I. A. and Pask, J. A., Stable and metastable equilibria in the system SiO_2–Al_2O_3; (phase diagrams for ceramists Vol. 6, Fig. 6443—system Al_2O_3–SiO_2). *Journal of the American Ceramic Society*, 1975, **58**, 507–512.
30. Sales, M. and Alarcon, J., Synthesis and phase transformation of mullites obtained from SiO_2–Al_2O_3 gels. *Journal of the European Ceramic Society*, 1996, **16**, 781–789.
31. Kingery, W. D., Plausible concepts necessary and sufficient for interpretation of ceramic grain-boundary phenomena: I. Grain-boundary characteristics, structure and electrostatic potential. *Journal of the American Ceramic Society*, 1974, **57**, 1–8.
32. Li, C.-W. and Kingery, W. D., Solute segregation at grain boundaries inpolycrystalline Al_2O_3 (In *Structure and Properties of MgO and Al_2O_3 Ceramics*, ed. W. D. Kingery). *Advances in Ceramics*, 1984, **10**, 368–378.
33. Lange, F. F., Sinterability of agglomerated powders. *Journal of the American Ceramic Society*, 1984, **67**, 83–89.